Original article

Gold-containing compound BDG-I inhibits the growth of A549 lung cancer cells through the deregulation of miRNA expression

Ali Alhoshani [a],[*], A. Alrashdi [a], Khaled Alhosaini [a], Fawaz E. Alanazi [a], Nehad M. Alajez [b], Muhammad Altaf [c], Anvarhusein A. Isab [d], Hesham M. Korashy [e]

[a] Department of Pharmacology and Toxicology, College of Pharmacy, King Saud University, Riyadh 11451, Saudi Arabia
[b] Stem Cell Unit, Department of Anatomy, College of Medicine, King Saud University, Riyadh 11461, Saudi Arabia
[c] Centre of Research Excellence in Nanotechnology (CENT), King Fahd University of Petroleum and Minerals, Dhahran 31261, Saudi Arabia
[d] Department of Chemistry, King Fahd University of Petroleum and Minerals, Dhahran 31261, Saudi Arabia
[e] Pharmaceutical Sciences Section, College of Pharmacy, Qatar University, Doha, Qatar

ARTICLE INFO

ABSTRACT

Gold complex bis(diethyldithiocarbamato-gold(I)) bis(diphenylphosphino) methane (BDG-I) is cytotoxic toward different cancer cell lines. We compared the cytotoxic effect of BDG-I with that of cisplatin in the A549 lung cancer cell line. Additionally, we investigated the molecular mechanism underlying the toxic effect of BDG-I toward the A549 cell line and the identification of cancer-related miRNAs likely to be involved in killing the lung cancer cells. Further, X-ray crystallographic data of the compound were acquired. Using microarray, global miRNA expression profiling in BDG-I-treated A549 cells revealed 64 upregulated and 86 downregulated miRNAs, which targeted 4689 and 2498 genes, respectively. Biological network connectivity of the miRNAs was significantly higher for the upregulated miRNAs than for the downregulated miRNAs. Two of the 10 most upregulated miRNAs (hsa-mir-20a-5p and hsa-mir-15b-5p) were associated with lung cancer. AmiGo2 server and Panther pathway analyses indicated significant enrichment in transcription regulation of miRNA target genes that promote intrinsic kinase-mediated signaling, TGF-β, and GnRH signaling pathways, as well as oxidative stress responses. BDG-I crystal structure X-ray diffraction studies revealed gold–gold intramolecular interaction [Au⋯Au = 3.1198 (3) Å] for a single independent molecule, reported to be responsible for its activity against cancer. Our present study sheds light on the development of novel gold complex with favorable anti-cancer therapeutic functionality.

1. Introduction

Lung cancer is the leading cause of cancer-associated deaths globally (Calin et al., 2004). Approximately 1.8 million new cases of lung cancer were reported worldwide in 2012 (Torre et al., 2015). According to American Cancer Society (ACS) estimates, there would be 234,030 new cases of lung cancer and approximately 154,050 deaths from the disease in the US in 2018(ACS, 2018). Lung malignancies can be either (a) non-small-cell lung cancer (NSCLC), which originates from the epithelial cells of the airways and accounts for about 85% of lung cancer cases, or (b) small-cell lung cancer, which is a neuroendocrine tumor. NSCLC is further categorized into several major histological subtypes, such as adenocarcinoma, squamous cell carcinoma, and large-cell carcinoma (Chin et al., 2008). The differential gene expression patterns observed in the different subtypes of lung cancer have a significant influence on the choice of chemotherapy drugs that could be used.

These expression patterns differ mainly because of the action of the existing tumor-specific microRNAs (miRNAs), which are endogenous non-coding RNA molecules of approximately 20–22 nucleotides in length. Since their discovery in 1993, more than 3700 human miRNAs have been identified (Londin et al., 2015). They modulate post-transcriptional gene expression by binding to the 3′ untranslated region of target messenger RNAs (mRNAs).

Each miRNA can regulate approximately 100–200 different mRNA targets (Krek et al., 2005; Lim et al., 2005). miRNAs downregulate the expression of a wide variety of genes involved in development, differentiation, proliferation, apoptosis, and various other crucial cellular processes.

Depending on the target mRNA, miRNAs may have oncogenic or tumor suppressor effects. The study by Calin et al. was one of the first to highlight the critical role played by miRNAs in lung cancer pathogenesis (Calin et al., 2004). Their study showed a decreased expression of several important miRNAs in lung cancer cell lines. Subsequently, Kumar et al. demonstrated that the *let-7* family of miRNAs acts as oncosuppressors in NSCLCs (Kumar et al., 2008). These results were in accordance with those of another study that showed a decreased expression of *let-7* miRNA in human NSCLCs (Takamizawa et al., 2004). In addition, this decreased expression of miRNA-16 in patients with NSCLC was found to be associated with an increased growth and motility of cancer cells (Ke et al., 2013). Taken together, these studies indicate that miRNAs could be used as novel therapeutic in lung cancer intervention.

The principles behind the development of chrysotherapeutic agents can be used to synthesize gold complexes that contain various functional ligands with distinctive pharmacological, chemical, physical, and biological properties (Bostancioglu et al., 2012; Al-Jaroudi, 2014). *In vitro* and *in vivo* studies have revealed that gold(I) and gold(III) complexes significantly impede cancer cell growth and hence can be used as an alternative to platinum-based anticancer drugs (Lima & Rodriguez, 2011; Che and Sun, 2011).

In the current decade, we have investigated the structural and antitumor properties of several gold(I) and gold(III) complexes of diamines, N-heterocyclic-carbenes, 2,2′-bipyridines, phosphines and dithiocarbamates ligands (Al-Jaroudi et al., 2017; Al-Jaroudi et al., 2014; Altaf et al., 2017; Muhammad Monim-ul-Mehboob, 2013). Based on our current studies and previous literature, it is well understood that the presence of dithiocarbamate ligands in phosphanegold(I) complexes improves their anticancer activity and selectivity for various carcinoma cells (Berners-Price & Filipovska, 2011; Humphreys et al., 2007). The antitumor activity of phosphine gold(I) complexes are found to be the function of phosphine substituent as well as the nature of the other auxiliary ligands present. The presence of dithiocarbamate group in gold(I) phosphine motifs prevents interaction of the metal center with sulfur-containing proteins, thereby reducing renal toxicity (Illan-Cabeza et al., 2013; Tian et al., 2011).

Our laboratory research focuses on the synthesis of novel gold complexes with anti-cancer therapy applications. Recently, we designed and synthesized a new compound, bis(diethyldithiocarbamato-gold(I)) bis(diphenylphosphino) methane (BDG-I), which is a complex of dithiocarbamate gold(I) with bisphosphine. This complex has been previously assessed for its apparent toxicity toward different cancer cell lines (Altaf et al., 2015). However, the molecular mechanism behind its cytotoxic effect is yet to be elucidated. Herein, we report the crystal structure of the BDG-I complex, as well as our investigation of its possible molecular mechanism of action against the A549 lung cancer cell line and identification of cancer-related miRNAs that might be mediating the effects.

2. Materials and methods

2.1. Chemicals and experimental conditions

All chemicals and solvents used in the synthesis of the gold(I) complex were of analytical grade. The reaction was carried out under ambient conditions, as described in our previous report (Altaf et al., 2015).

2.2. Cell culture and viability assay

The human A549 lung cancer cell line was purchased from the American Type Culture Collection (ATCC, USA). The A549 cells were first cultured for 24 h in 96-well plates, at 5×10^4 cells/well (in quadruplicate), in 150 μL of Dulbecco's modified Eagle's medium (DMEM). Subsequently, the cells were incubated with BDG-I at 0 (negative control), 1.56, 3.12, 6.25, 12.5, 25, 50, and 100 μM concentrations for 48 h in DMEM, containing 10% fetal bovine serum (FBS) and 1% penicillin/streptomycin, under 5% CO_2 at 37 °C and 95% relative humidity. Thereafter, the medium in each well was discarded, then 100 μL of DMEM containing 5 mg/mL 3-(4,5-dimethylthiazol-2-yl)-2,5-diphenyltetrazolium bromide (MTT) was added to the wells, and the plates were placed in a CO_2 incubator at 37 °C for 4 h. After incubation, purple-colored formazan was produced and appeared as dark crystals at the bottom of the wells. The culture medium was carefully discarded from each well to avoid disruption of the monolayer, followed by the addition of 100 μL isopropanol to each well. The solution was mixed thoroughly to dissolve the formazan crystals, which ultimately resulted in a purple solution. The absorbance of each solution in the 96-well plate was measured at 570 nm (Mithras 2 LB 943 system) against a reagent blank. The percentage of cell viability was calculated with the following formula:

$$\text{Cell viability} \% = 100 \times (\text{Absorbance}_{\text{Compound}})/(\text{Absorbance}_{\text{DMSO}})$$

The IC_{50} value was calculated for each sample, using GraphPad 6.0 and Excel 2016.

2.3. Total RNA extraction and miRNA expression profiling

A549 cells were cultured in 6-well plates at 5×10^5 cells/well (in duplicate) for 24 h. The cells were then treated for 48 h with either BDG-I at IC_{50} concentration or medium (negative control). Thereafter, the cells were harvested and the cell pellets were prepared for total RNA isolation, using the Total RNA Purification Kit (Norgen Biotek Corp., Canada), according to the manufacturer's protocol. The concentration of total RNA (including miRNA fraction) for each sample was measured, using the NanoDrop 2000 spectrophotometer (Thermo Fisher Scientific, USA). For miRNA expression profiling, 100 ng of the extracted total RNA was used for RNA labeling and hybridization onto the Agilent Human SurePrint G3 8×60 k v.21 miRNA microarray chip (Agilent Technologies, USA), according to the manufacturer's protocol. Subsequently, the data were normalized and analyzed using GeneSpring GX software (Agilent Technologies). A fold-change (FC) of 2.0 with p < 0.05 was used as the cut-off for determining the differentially expressed miRNAs in treated versus control samples.

2.4. Target prediction and functional analysis of miRNA target genes

We used miRWalk2 (http://zmf.umm.uniheidelberg.de/apps/zmf/mirwalk2/) to identify target genes of the upregulated and downregulated miRNAs (Dweep and Gretz, 2015). Targeted genes of the miRNAs were analyzed for Gene Ontology (GO) term enrichment using the AmiGO2 server (v.1.8), based on the Panther database (Carbon et al., 2009).

2.5. miRNA and gene (target) regulatory network

2.5.1. Global network representation of upregulated and downregulated genes

All differentially expressed miRNAs and their target genes were considered for construction of a miRNA-gene regulatory

network, drawn using Cytoscape 3.5.1 (Shannon et al., 2003), and were represented as unweighted and undirected. Generally, upregulated genes have a high degree of interaction with their target genes in a dense network relative to that shown by downregulated genes.

2.5.2. Top 10 miRNAs and target gene regulatory network

All differentially expressed miRNAs were ranked on the basis of total interactions with their target genes (Wu et al., 2017). The top 10 miRNAs and their respective targets were used for network illustration in Cytoscape 3.5.1. For better visualization, we chose only those miRNAs with a degree of interaction ≥ 2. As the downregulated genes had a connection of <2, they were disregarded.

2.6. Illustration of miRNAs involved in lung cancer

The miRCancer database (http://mircancer.ecu.edu) (Xie et al., 2013) was used to detect the role of miRNAs in lung cancer. Out of 20 miRNA genes (up/downregulated), two (hsa-miR-20a-5p, hsa-miR-15b-5p) were upregulated and were involved in lung cancer. Both these miRNAs and their respective target genes were illustrated in our network using Cytoscape 3.5.1.

2.7. X-ray crystallography

X-ray diffraction data for the BDG-I complex were recorded on a Bruker AXS SMART APEX detector (Bruker AXS Inc., USA), equipped with graphite-monochromated MoKα radiation ($\lambda = 0.71073$ Å). The data were collected and integrated using SMART (v.5.05) software for the SMART APEX system. The data integration was performed using SAINT. Empirical absorption correction was carried out using SADABS (Sheldrick, 1996). The structure was solved with direct methods and refined by full-matrix least-squares based on F^2, using the structure determination package based on SHELX 97 software (SHELXTL v.5.1; Bruker AXS Inc.). Graphics were generated using ORTEP-3 (Farrugia, 1997). With the help of a riding model, other H-atoms were included in the calculated positions. The crystal data and structure refinement details are displayed in Tables 1 and 2.

Table 1
Crystal data and structure refinement details of the BDG-I complex.

Crystal data	
Empirical formula	$C_{35}H_{42}Au_2N_2P_2S_4$
Formula weight	1074.82
Crystal system, space group	Monoclinic, P 2_1/c
Temperature (K)	296 (2)
a, b, c (Å)	12.6361 (12), 12.9532 (12),
β (°)	23.215 (2)
V (Å^3)	91.988 (2)
Z	3797.5 (6)
Radiation type	4
μ (mm^{-1})	Mo Kα
Crystal size (mm)	8.049
Absorption correction	0.31 × 0.26 × 0.15
T_{min}, T_{max}	Multiscan
No. of measured, independent, and	0.127, 0.378
observed	27052, 9421, 6935
[$I > 2\sigma(I)$] reflections	
R_{int}	0.043
$(\sin \theta/\lambda)_{max}$ (Å^{-1})	0.667
$R[F^2 > 2\sigma(F^2)]$, $wR(F^2)$, S	0.033, 0.082, 1.00
No. of reflections	9421
No. of parameters	410
$\Delta\rho_{max}$, $\Delta\rho_{min}$ (e Å^{-3})	1.11, −1.14

Table 2
Selected bond lengths (Å) and bond angles (°) of the BDG-I complex.

Bond length (Å)		Bond angles (°)	
Au1-P1	2.2546 (12)	P1-Au1-S1	170.93 (5)
Au2-P2	2.2660 (12)	P2-Au2-S3	170.68 (5)
Au1-S1	2.3365 (13)	P1-Au1-Au2	84.31 (3)
Au2-S3	2.3324 (14)	S1-Au1-Au2	90.44 (3)
Au1-Au2	3.1198 (3)	P2-Au2-Au1	87.82 (3)
		S3-Au2-Au1	95.09 (4)

2.8. Statistical analysis

R statistical tools version 3.2 was used for all statistical tests in miRNAs network analysis. We used statistical tests (Mood's Test) for network connectivity to show the changes in network structure between upregulated and downregulated miRNA. And a nonparametric test (Wilcoxon Rank Sum Test) to show the differences in mean connectivity between the two networks (Team, 2013).

3. Results and discussion

3.1. Cell viability

We assessed the inhibition of A549 cell growth upon exposure to various concentrations of BDG-I by MTT assay. BDG-I inhibited the cell growth in a dose-dependent manner (Fig. 1), with an IC$_{50}$ value of 4.8 μM. Of note, the IC$_{50}$ value of BDG-I was better than that of cisplatin (IC$_{50}$ = 8.5 μM).

3.2. miRNA analysis

Global miRNA expression profiling in BDG-I-treated A549 cells revealed 64 upregulated (>2.0 FC, p < 0.05) and 86 downregulated (<2.0 FC, p < 0.05) miRNAs targeting 4689 and 2498 genes, respectively. Hierarchical clustering of the differentially expressed miRNAs revealed a clear separation of the two groups (Fig. 2). We disregarded genes targeted by only one miRNA because these are likely to be random signals.

3.3. Network analysis of differentially expressed miRNAs and their targets

3.3.1. Network connectivity of upregulated and downregulated miRNAs

The levels of interconnectivity between the miRNAs and their target genes were analyzed. The density plots (Fig. 3) suggested
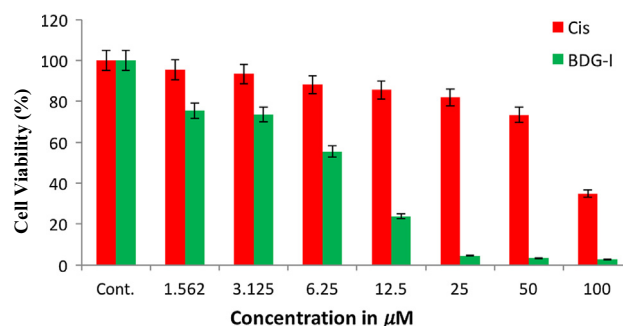

Fig. 1. Inhibitory effects of BDG-I and cisplatin (Cis) on A549 cell line growth in a dose-dependent manner. A549 cells were cultured in a 96-well plate at a density of 5×10^4 cells/well. BDG-1 or cisplatin was added to the cells various concentration. DMEM was used in untreated cells as a control. Subsequently, MTT assay was performed, and the degree of cell proliferation was measured at 570 nm, followed by determination of percent cell viability. Data are presented as a bar graph for comparison of cell proliferation.
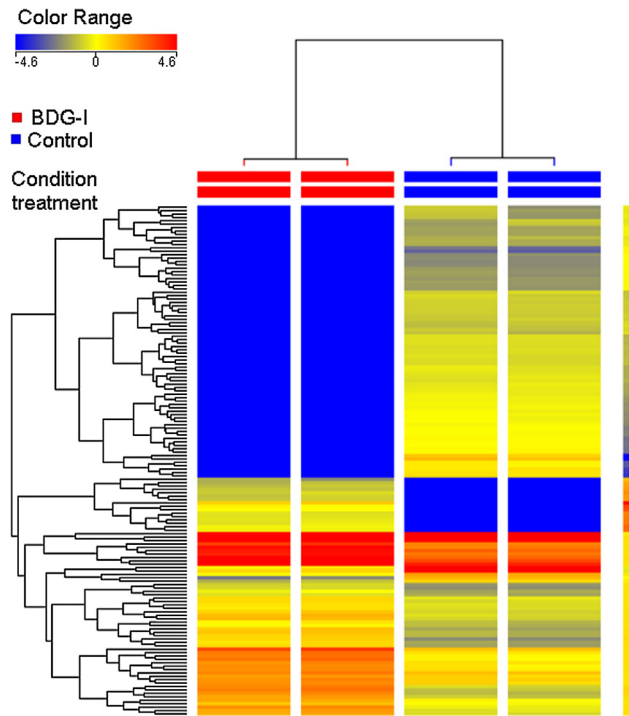
Fig. 2. miRNA expression profiling in BDG-I-treated A549 cells. Hierarchical clustering of A549 cells treated with BDG-I or DMSO (control), based on miRNA expression levels. Each column represents a replica, and each row represents a miRNA. The expression level of each miRNA in a single sample is depicted according to the color scale.

that most of the miRNAs had multiple targets. The median number of gene targets was 236 and 81 for the upregulated and downregulated miRNAs, respectively. Such high median target numbers suggested that the treatment applied had widespread effects on the cellular system. It is clear from Fig. 3 that the connectivity of the miRNAs (genes or targets per miRNA) was significantly higher for the upregulated miRNAs than for the downregulated miRNAs.

The network components were quantified miRNA-wise and gene target-wise, as shown in Fig. 4. The difference between the mean connectivity between genes (Fig. 4; left panels) was statistically significant ($P_{Wilcox} < 2.2E{-}16$). This difference can be attributed to the difference in the scales of connectivity between the two groups of genes ($P_{Mood} < 2.2E{-}16$). Although non-parametric and scale tests showed a significant difference in connectivity, there was no perceptible difference in the medians between the two groups (Fig. 4; median difference = 0). The box plot for miRNA-wise connectivity (Fig. 4; right panel) showed that a typical upregulated miRNA was likely to regulate more genes than a typical downregulated miRNA. These differences were statistically significant ($P_{Wilcox} = 1.39E{-}05$). The Mood's median test also showed a significant difference between the scales of networks of the upregulated and downregulated miRNAs ($P_{Mood} = 0.002$).

3.4. Biological network structure of differentially expressed miRNAs

Next, we studied the networks of the upregulated and downregulated miRNAs. As was expected from the connectivity statistics, the upregulated miRNAs had a densely interconnected network. Not only were they regulating more genes, but there was also a high degree of interconnectivity. We ranked each miRNA by the number of genes it targeted and created a network illustration of the top 10 miRNAs (Fig. 5). These target genes were actively and collectively regulated by several of the selected top 10 miRNAs.

Many of the genes were regulated by more than 2 of the top 10 miRNAs. Such network structure suggests a core biological function being targeted by the top miRNAs (Aittokallio and Schwikowski, 2006). This level of interconnectedness was in stark contrast to the network structure of the downregulated miRNAs, which was much less interconnected (Fig. 6). In Fig. 6, the same measurement criteria were employed for the upregulated miRNAs (Fig. 5; top 10 most connected miRNA + genes that have at least two connections within this group) but two were dropped because none of their target genes had a connectedness of 2 within this group. It could be seen from Fig. 6 a sparser network for the downregulated miRNA and their targets.

3.5. Network architecture of the upregulated miRNAs and their target genes

Given the network density of the upregulated miRNAs and its significant variance from that of the downregulated miRNAs, we questioned whether the density was merely because of a large number of targets possessed by each upregulated miRNA. To elucidate this, we calculated the closeness centrality, which measures how close a given node is to the others in the network. In our analysis, closeness centrality provides a measure of the interconnectedness and coregulation of the genes by the miRNA in question (Koschutzki and Schreiber, 2008); (Reuven Cohen, 2003). Fig. 7 compares the closeness centrality of upregulated and downregulated genes in their respective networks. It showed that there were two distinct networks – one whose closeness centrality behaves in the random fashion (the set of dots that lie along the diagonal), and another where the closeness increases without an increase in the number of neighbors. This atypical behavior of the up-regulated network provides a quantitative measurement of interconnectedness shown in Fig. 5. The analysis also suggested that the upregulated miRNA -target gene network [Fig. 7, left panel] behaved as a mixture of two distinct groups: one that behaved in a random fashion, and another closely linked network that is likely to be functionally significant. A random network is expected to follow an exponential decay function, where the closest mean distance increases as we increase the number of neighbors (Reuven Cohen, 2003). The closeness centrality analysis reveals that the downregulated network [Fig. 7, right panel] behaves as we expect from a typical biological network with random connectivity (Reuven Cohen, 2003). However, the network of upregulated miRNA and their target genes exhibits an interesting behavior.

3.6. miRNA network in lung cancer

Given the strong differences between the upregulated and downregulated miRNAs and their network densities, we questioned whether any of these had a documented role in lung cancer and if any of the top 10 upregulated and downregulated miRNAs were also listed in the miRCancer Database (http://mircancer.ecu.edu). Two of the 10 upregulated miRNAs (hsa-mir-20a-5p and hsa-mir-15b-5p) were indeed found to be associated with lung cancer. These two miRNAs had a complement of 27 coregulated genes. Interestingly, functional analysis of these genes did not reveal any lung cancer-related miRNAs in the top 10-downregulated miRNAs (Fig. 8). At least three transcription factors (Homeobox Containing 1 "HMBOX1", The DEAD-box-protein "DDX5", Zinc Finger and BTB Domain Containing 5 "ZBTB5") were identified to be coregulated by the two miRNAs. All of these transcription factors have implication on cancer progression (Koh et al., 2009; Ma et al., 2015; Wang et al., 2015). The presence of transcription factors in the network suggested that the miRNA differential expression would have downstream secondary effects, apart from direct effects on their targets (Fig. 8). Therefore, these
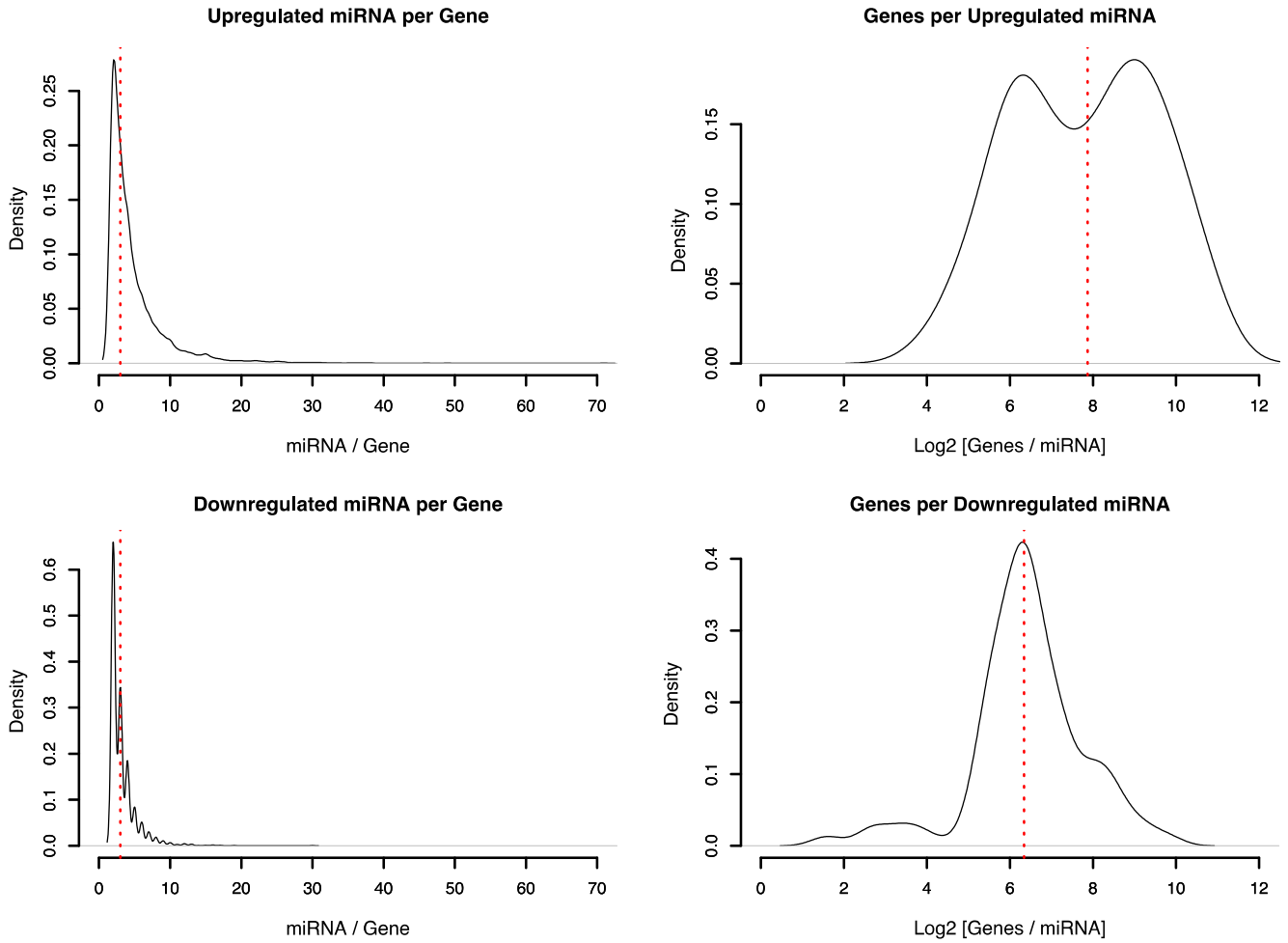
Upregulated miRNA per Gene

Genes per Upregulated miRNA

Downregulated miRNA per Gene

Genes per Downregulated miRNA

Fig. 3. Density distribution of the connectivity of the miRNA/gene interaction network. The panels illustrate the degree of connectivity in terms of genes (left panels) and miRNAs (right panels). The X-axis for the panels on the right is depicted in Log2 scale. The red vertical lines indicate the median connectedness values for each group.
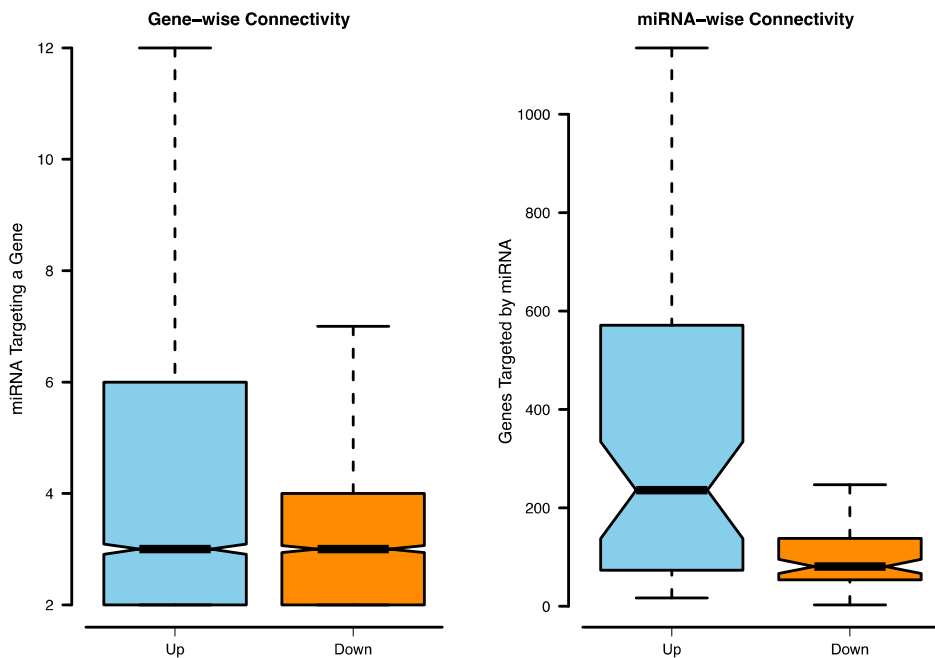
Gene–wise Connectivity

miRNA–wise Connectivity

Fig. 4. Network connectivity for the upregulated and downregulated miRNAs and gene targets in A549 lung cancer cells. The blue and orange colors represent the relatively upregulated and downregulated expression, respectively. Gene-wise connectivity (left graph), miRNA-wise connectivity (right graph). As the degree of connectivity of a gene gets higher, the node within the network gets larger.
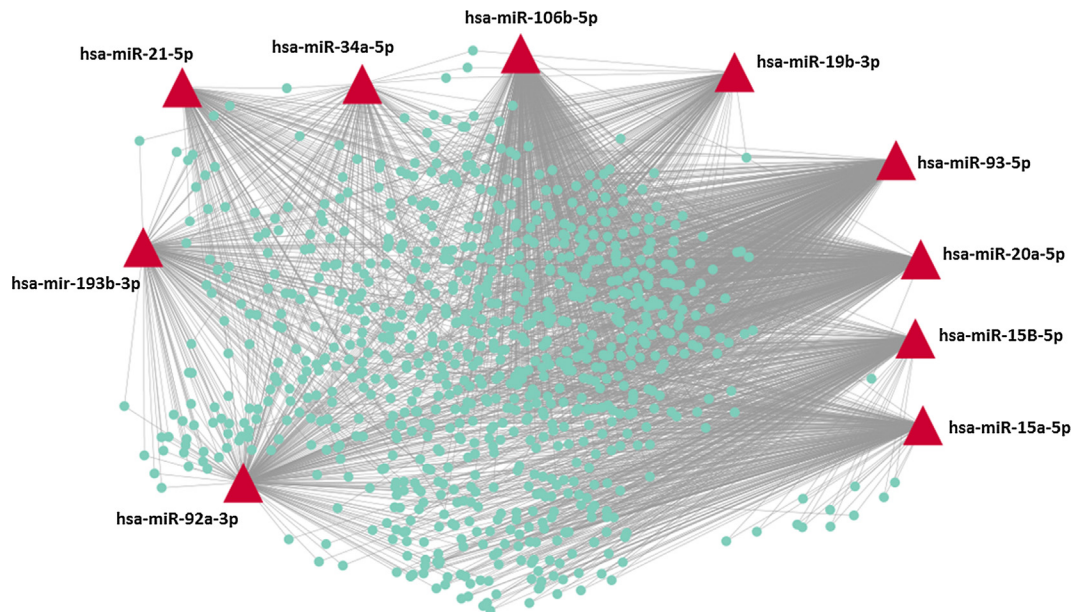
Fig. 5. A network of the top 10 upregulated miRNAs (depicted by red triangles) and their target genes (depicted by green dots). The miRNAs were named according to standard nomenclature.
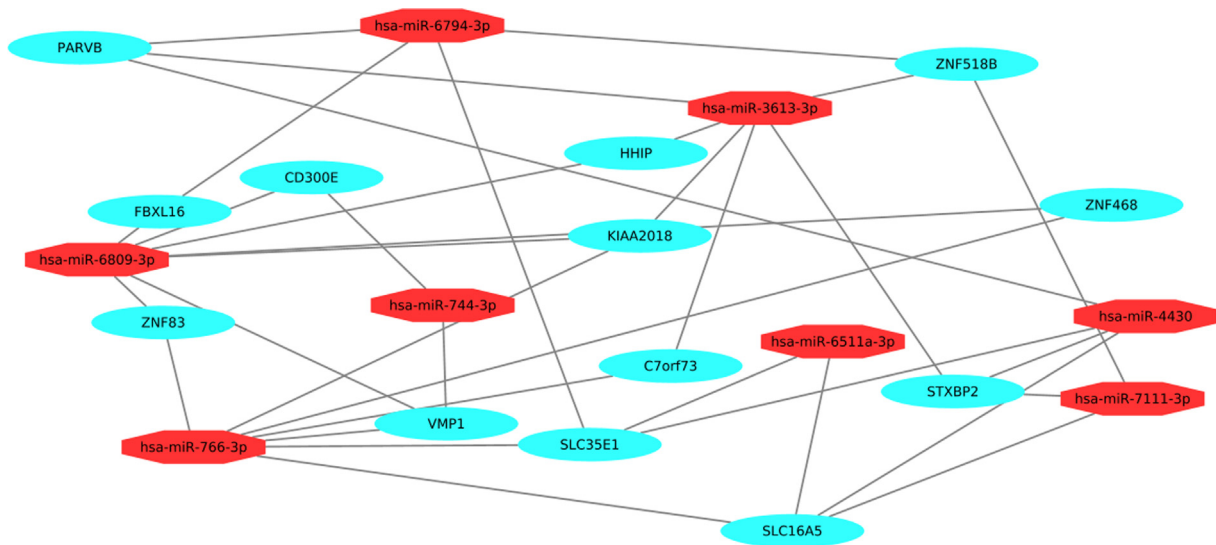

Fig. 6. A network of the top downregulated miRNAs (depicted by red octagons) and their target genes (depicted by green ovals).

transcription factors and their secondary effect could be a potential therapeutic target.

3.7. Functional analysis of miRNA target genes

The gene interaction networks for the upregulated and downregulated miRNAs suggested a strong functional implication for the upregulated miRNAs. To test this hypothesis, we performed GO term enrichment and pathway enrichment analyses on the targets of the upregulated and downregulated miRNAs. We identified the unique set of genes regulated by the up and downregulated miRNAs and performed a GO term enrichment analysis on the AmiGO2 server (Ashburner et al., 2000), based on the PantherDB (Table 3) (Mi et al., 2017).

Several terms associated with protein kinase activity were over-represented, whereas receptor activity and *G protein*-coupled

receptor (GPCR) activity were underrepresented. This suggested an enrichment of miRNA gene targets that drive intrinsic kinase-mediated signaling and a lack of targets that drive receptor-mediated signaling. Notably, GPCR signaling was also underrepresented in our Reactome Pathway analysis, suggesting that GPCR-based signaling was likely not selectively targeted in this study.

Next, we analyzed the pathways that are likely affected by changes in miRNA expression, using Panther Pathways to identify enriched or depleted pathways (Table 4). Genes were found to be enriched in angiogenesis, the transforming growth factor-beta (TGF-β) pathway, the cholecystokinin receptor pathway, the platelet-derived growth factor pathway, the gonadotropin-releasing hormone pathway, and oxidative stress response. The target gene set was enriched for all these pathways, and no depleted pathways were identified. It is clear that all identified pathways play an important role in cancer.
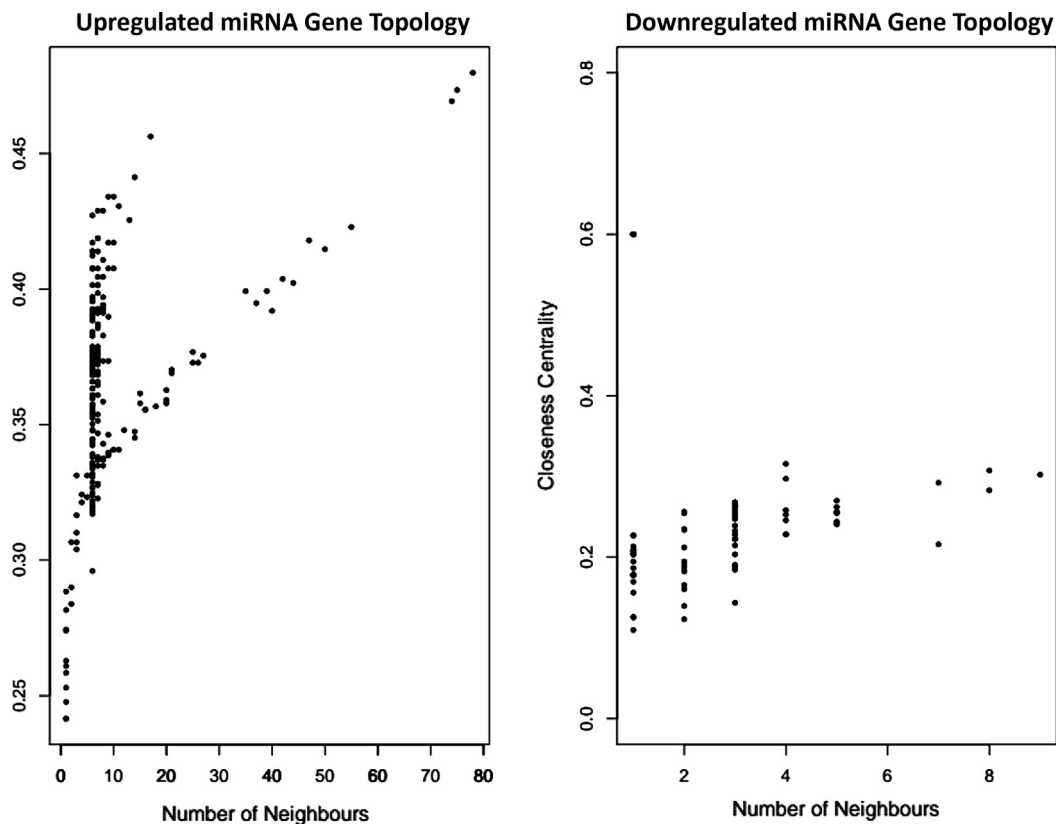
Fig. 7. Closeness centrality of the miRNA networks. The graphs illustrate the correlation between closeness, and the number of neighbors within the network.
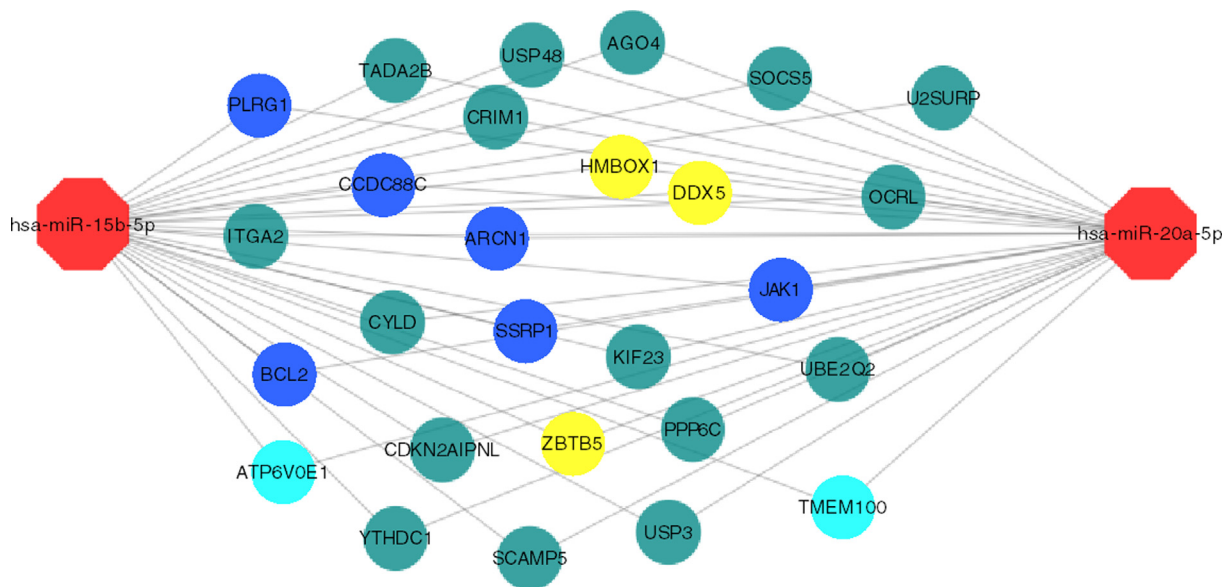

Fig. 8. Coregulated genes of hsa-mir-20a-5p and hsa-mir-15b-5p. The figure illustrates the interconnected nature of miRNA regulation in lung cancer. The red octagons represent the miRNAs, yellow circles represent transcription factors, blue circles represent plasma proteins, cyan circles represent membrane proteins, and green circles represent intracellular genes.

We did not find any enriched pathways or GO terms for the target genes of downregulated miRNAs. This supported the conclusion from the networks that the miRNA response is directional, and it is likely that the upregulated miRNAs are more biologically relevant.

3.8. Description of the BDG-I complex structure

The dinuclear structures of the BDG-I complex were confirmed by X-ray diffraction studies (Fig. 9). A selection of bond lengths and bond angles are given in Table 2. The BDG-I complex crystallizes in

Table 3
GO-Slim analysis of targets of upregulated miRNAs.

PANTHER GO-slim molecular function	Human RefLIST	Test gene count	Test gene expected	Enrichment	Fold enrichment	P-value
protein kinase activity (GO:0004672)	406	68	38.45	+	1.77	1.48E−03
kinase activity (GO:0016301)	573	87	54.27	+	1.6	3.46E−03
enzyme regulator activity (GO:0030234)	678	99	64.21	+	1.54	4.31E−03
transferase activity (GO:0016740)	1318	180	124.82	+	1.44	1.57E−04
catalytic activity (GO:0003824)	4708	587	445.87	+	1.32	2.15E−11
hydrolase activity (GO:0016787)	1934	233	183.16	+	1.27	1.91E−02
nucleic acid binding (GO:0003676)	2080	249	196.99	+	1.26	1.60E−02
binding (GO:0005488)	5024	559	475.8	+	1.17	1.70E−03
Unclassified (UNCLASSIFIED)	10,950	908	1037.02	−	0.88	0.00E+00
receptor activity (GO:0004872)	1279	60	121.13	−	0.5	3.69E−08
signal transducer activity (GO:0004871)	715	27	67.71	−	0.4	1.79E−06
G-protein coupled receptor activity (GO:0004930)	350	12	33.15	−	0.36	3.52E−03

Table 4
Panther Pathway analysis of targets of upregulated miRNAs.

PANTHER pathways	Human RefLIST	Test gene count	Test gene expected	Enrichment	Fold enrichment	P-value
Oxidative stress response (P00046)	55	18	5.21	+	3.46	1.43E−03
TGF-beta signaling pathway (P00052)	98	26	9.28	+	2.8	7.49E−04
CCKR signaling map (P06959)	173	45	16.38	+	2.75	5.74E−07
PDGF signaling pathway (P00047)	149	31	14.11	+	2.2	1.03E−02
GRH receptor pathway (P06664)	236	47	22.35	+	2.1	5.02E−04
Angiogenesis (P00005)	174	34	16.48	+	2.06	1.54E−02

a monoclinic lattice with space group P 2₁/c. The asymmetric unit consists of a single molecule. The [Au-P = 2.2546 (12) and 2.2660 (12) Å] and [Au-S = 2.3365 (13) and 2.3324 (14) Å] bond distances are typical for this type of complex (Arias et al., 2008; Fernandez et al., 1998; Altaf et al., 2015). The dithiocarbamate ligand acts as a monodentate ligand in this dinuclear gold(I) complex. The P-Au-S bond angles (170.93 (5) and 170.68 (5)°) confirm a distorted linear geometry around the Au1 and Au2 atoms. The presence of this type of distorted geometry around gold atoms is consistent with that of reported gold complexes possessing a similar P-Au-S moiety (Arias et al., 2008; Fernandez et al., 1998; Altaf et al., 2015). The intramolecular Au-Au distance of 3.1198 (3) Å for Au1-Au2 indicates metal–metal interaction. The diphosphine adopts a *cis* conformation, with Au1-P1···P2-Au2 = 29.51°, which shows that the P-Au-S moiety is twisted. The *cis* conformation is usually preferred over the *trans* conformation, owing to Au-Au interaction.
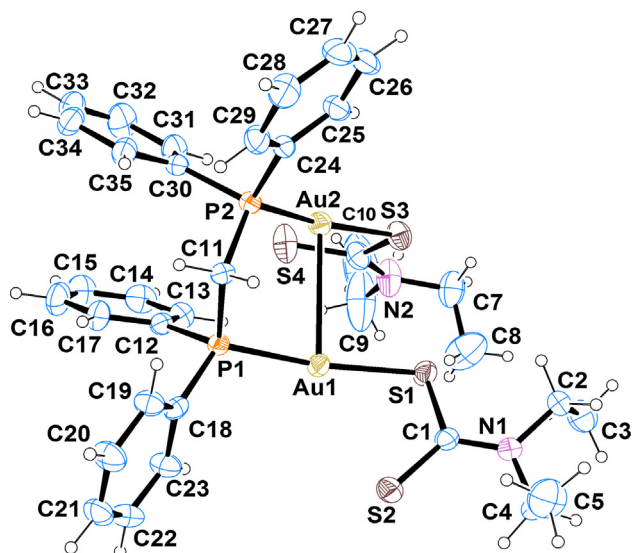

Fig. 9. Crystal structure of BDG-I, showing the atom labeling scheme and displacement ellipsoids at the 50% probability level.

4. Conclusion

In summary, BDG-1 exhibited anti-cancer functionality and displayed a much better potency, than cisplatin, and altered miRNAs expression profile in A549 lung cancer cells. We constructed a biological network of miRNA and gene targets for up and downregulated miRNAs. These network frameworks can exploit modularity in terms of interconnectivity and biological relevance with target genes. In case of upregulated miRNA-gene network, 64 miRNAs and 4689 targets were used for the construction of network while 86 miRNAs and 2498 targets were used in case of downregulated miRNA. It could be inferred from the analysis that there is directionality to miRNA response and an upregulated miRNA are biologically more relevant and have dense connectivity with their respective target genes. We also documented the role of miRNA in lung cancer and two [hsa-mir20a-5p and hsa-mir-15b-5p] of 10 top upregulated miRNA genes were found to be associated with lung cancer which has 27 coregulated genes. The presence of transcription factors in the lung cancer network also suggests that the miRNA differential expression would have downstream secondary effects, apart from their direct effect on their targets. Thus, miRNA-gene network study suggests upregulated miRNA are biologically more relevant. The X-ray structure of BDG-1 complex reveals that it is a binuclear gold(I) complex with a P-Au-S moiety. In this complex, a very important and exploitable property of intermolecular aurophilic interaction was observed. The enhanced activity of the BDG-1 complex was attributed to aurophilic interaction in this study. Thus, our current study shows that the BDG-1 treatment affects the micro-RNA network, and is a strong disruptor of basic cellular mechanisms in lung cancer cell lines and provides insight into the importance of the development of new gold(I) complexes and the elucidation of their potential as novel anti-cancer therapeutic agents. Future work will focus on the mechanistic nature of the effect, and its possible implications for the clinic.

References

ACS, 2018. American Cancer Society Retrieved from https://www.cancer. org/cancer/non-small-cell-lung-cancer/about/key-statistics.html, .

Aittokallio, T., Schwikowski, B., 2006. Graph-based methods for analysing networks in cell biology. Brief. Bioinform. 7 (3), 243–255. https://doi.org/10.1093/bib/bbl022.

Al-Jaroudi, S.S., Altaf, M., Seliman, A.A., Yadav, S., Arjmand, F., Alhoshani, A., Korashy, H.M., Ahmad, S., Isab, A.A. (2017). Synthesis, characterization, in vitro cytotoxicity and DNA interaction study of phosphanegold(I) complexes with dithiocarbamate ligands. Inorg. Chim. Acta, 464, 37–48.

Al-Jaroudi, S.S., Monim-ul-Mehboob, M., Altaf, M., Al-Saadi, A.A., Wazeer, M.I., Altuwaijri, S., Isab, A.A., 2014. Synthesis, spectroscopic characterization, electrochemical behavior and computational analysis of mixed diamine ligand gold(III) complexes: antiproliferative and in vitro cytotoxic evaluations against human cancer cell lines. Biometals 27 (6), 1115–1136. https://doi.org/10.1007/s10534-014-9771-2.

Altaf, M., Monim-Ul-Mehboob, M., Kawde, A.N., Corona, G., Larcher, R., Ogasawara, M., Isab, A.A., 2017. New bipyridine gold(III) dithiocarbamate-containing complexes exerted a potent anticancer activity against cisplatin-resistant cancer cells independent of p53 status. Oncotarget 8 (1), 490–505. https://doi.org/10.18632/oncotarget.13448.

Arias, J., Bardají, M., Espinet, P., 2008. Mononuclear, dinuclear, and hexanuclear gold (I) complexes with (aza-15-crown-5) dithiocarbamate. Inorg. Chem. 47 (5), 1597–1606.

Ashburner, M., Ball, C.A., Blake, J.A., Botstein, D., Butler, H., Cherry, J.M., Sherlock, G., 2000. Gene ontology: tool for the unification of biology. The Gene Ontology Consortium. Nat. Genet. 25 (1), 25–29. https://doi.org/10.1038/75556.

Berners-Price, S.J., Filipovska, A., 2011. Gold compounds as therapeutic agents for human diseases. Metallomics 3 (9), 863–873. https://doi.org/10.1039/c1mt00062d.

Bostancioglu, R.B., Isik, K., Genc, H., Benkli, K., Koparal, A.T., 2012. Studies on the cytotoxic, apoptotic and antitumoral effects of Au(III) and Pt(II) complexes of 1, 10-phenanthroline on V79 379A and A549 cell lines. J. Enzyme. Inhib. Med. Chem. 27 (3), 458–466. https://doi.org/10.3109/14756366.2011.596835.

Calin, G.A., Sevignani, C., Dumitru, C.D., Hyslop, T., Noch, E., Yendamuri, S., Croce, C. M., 2004. Human microRNA genes are frequently located at fragile sites and genomic regions involved in cancers. Proc. Natl. Acad. Sci. USA 101 (9), 2999–3004. https://doi.org/10.1073/pnas.0307323101.

Carbon, S., Ireland, A., Mungall, C.J., Shu, S., Marshall, B., Lewis, S., AmiGO Hub and Web Presence Working, G. (2009). AmiGO: online access to ontology and annotation data. Bioinformatics, 25(2), 288–289. http://doi.org/10.1093/bioinformatics/btn615

Chin, L.J., Ratner, E., Leng, S., Zhai, R., Nallur, S., Babar, I., Weidhaas, J.B., 2008. A SNP in a let-7 microRNA complementary site in the KRAS 3′ untranslated region increases non-small cell lung cancer risk. Cancer Res. 68 (20), 8535–8540. https://doi.org/10.1158/0008-5472.CAN-08-2129.

Dweep, H., Gretz, N., 2015. miRWalk2.0: a comprehensive atlas of microRNA-target interactions. Nat. Methods 12 (8), 697. https://doi.org/10.1038/nmeth.3485.

Farrugia, L.J., 1997. ORTEP-3 for Windows-a version of ORTEP-III with a Graphical User Interface (GUI) (565-565) J. Appl. Crystallogr. 30 (5), 565.

Fernandez, E.J., Lopez-de-Luzuriaga, J.M., Monge, M., Olmos, E., Gimeno, M.C., Laguna, A., Jones, P.G., 1998. Dithiocarbamate ligands as building-blocks in the coordination chemistry of gold. Inorg. Chem. 37 (21), 5532–5536.

Humphreys, A.S., Filipovska, A., Berners-Price, S.J., Koutsantonis, G.A., Skelton, B.W., White, A.H. (2007). Gold(I) chloride adducts of 1,3-bis(di-2-pyridylphosphino) propane: synthesis, structural studies and antitumour activity. Dalton Trans. (43), 4943–4950. http://doi.org/10.1039/b705008a

Illan-Cabeza, N.A., Garcia-Garcia, A.R., Martinez-Martos, J.M., Ramirez-Exposito, M. J., Pena-Ruiz, T., Moreno-Carretero, M.N., 2013. A potential antitumor agent, (6-amino-1-methyl-5-nitrosouracilato-N3)-triphenylphosphine-gold(I): structural studies and in vivo biological effects against experimental glioma. Eur. J. Med. Chem. 64, 260–272. https://doi.org/10.1016/j.ejmech.2013.03.067.

Ke, Y., Zhao, W., Xiong, J., Cao, R., 2013. Downregulation of miR-16 promotes growth and motility by targeting HDGF in non-small cell lung cancer cells. FEBS Lett. 587, 3153–3157.

Koh, D.I., Choi, W.I., Jeon, B.N., Lee, C.E., Yun, C.O., Hur, M.W., 2009. A novel POK family transcription factor, ZBTB5, represses transcription of p21CIP1 gene. J. Biol. Chem. 284 (30), 19856–19866. https://doi.org/10.1074/jbc.M109.025817.

Koschutzki, D., Schreiber, F., 2008. Centrality analysis methods for biological networks and their application to gene regulatory networks. Gene. Regul. Syst. Biol. 2, 193–201.

Krek, A., Grun, D., Poy, M.N., Wolf, R., Rosenberg, L., Epstein, E.J., Rajewsky, N., 2005. Combinatorial microRNA target predictions. Nat. Genet. 37 (5), 495–500. https://doi.org/10.1038/ng1536.

Kumar, M.S., Erkeland, S.J., Pester, R.E., Chen, C.Y., Ebert, M.S., Sharp, P.A., Jacks, T., 2008. Suppression of non-small cell lung tumor development by the let-7 microRNA family. Proc. Natl. Acad. Sci. USA 105 (10), 3903–3908. https://doi.org/10.1073/pnas.0712321105.

Lim, L.P., Lau, N.C., Garrett-Engele, P., Grimson, A., Schelter, J.M., Castle, J., Johnson, J. M., 2005. Microarray analysis shows that some microRNAs downregulate large numbers of target mRNAs. Nature 433 (7027), 769–773. https://doi.org/10.1038/nature03315.

Lima, J.C., Rodriguez, L., 2011. Phosphine-gold(I) compounds as anticancer agents: general description and mechanisms of action. Anticancer Agents Med. Chem. 11 (10), 921–928.

Londin, E., Loher, P., Telonis, A.G., Quann, K., Clark, P., Jing, Y., Rigoutsos, I., 2015. Analysis of 13 cell types reveals evidence for the expression of numerous novel primate- and tissue-specific microRNAs. Proc. Natl. Acad. Sci. USA 112 (10), E1106–E1115. https://doi.org/10.1073/pnas.1420955112.

Ma, H., Su, L., Yue, H., Yin, X., Zhao, J., Zhang, S., Miao, J., 2015. HMBOX1 interacts with MT2A to regulate autophagy and apoptosis in vascular endothelial cells. Sci. Rep. 5, 15121. https://doi.org/10.1038/srep15121.

Mi, H., Huang, X., Muruganujan, A., Tang, H., Mills, C., Kang, D., Thomas, P.D., 2017. PANTHER version 11: expanded annotation data from Gene Ontology and Reactome pathways, and data analysis tool enhancements. Nucleic Acids Res. 45 (D1), D183–D189. https://doi.org/10.1093/nar/gkw1138.

Altaf, M., Monim-ul-Mehboob, M., Isab, A.A., Dhuna, V., Bhatia, G., Dhuna, K., Altuwaijri, S. (2015). The synthesis, spectroscopic characterization and anticancer activity of new mono and binuclear phosphanegold(I) dithiocarbamate complexes. New J. Chem. (1).

Muhammad Monim-ul-Mehboob, M.A., Fettouhi, Mohammed, Isab, Anvarhusein A., Wazeer, Mohammed I.M., Nasiruzzaman Shaikh, M., Altuwaijri, Saleh, 2013. Synthesis, spectroscopic characterization and anti-cancer properties of new gold (III)–alkanediamine complexes against gastric, prostate and ovarian cancer cells; crystal structure of [Au2(pn)2(Cl)2]Cl2.H2O]. Polyhedron 61, 225–234.

Reuven Cohen, S.H., Daniel ben-Avraham. (2003). Structural properties of scale-free networks. In: Stefan Bornholdt, H.G.S. (Ed.), Handbook of Graphs and Networks: From the Genome to the Internet (vol. 1): Wiley-VCH Verlag GmbH & Co. KGaA.

Al-Jaroudi, S.S., Monim-ul-Mehboob, M., Altaf, M., Fettouhi, M., Wazeer, M.I., Altuwaijri, S., Isab, A.A. (2014). Synthesis, spectroscopic characterization, X-ray structure and electrochemistry of new bis(1,2-diaminocyclohexane)gold(III) chloride compounds and their anticancer activities against PC3 and SGC7901 cancer cell lines. New J. Chem., 38(7). http://doi.org/10.1039/C3NJ01624B

Shannon, P., Markiel, A., Ozier, O., Baliga, N.S., Wang, J.T., Ramage, D., Ideker, T., 2003. Cytoscape: a software environment for integrated models of biomolecular interaction networks. Genome Res. 13 (11), 2498–2504. https://doi.org/10.1101/gr.1239303.

Sheldrick, G. (1996). Program for empirical absorption correction of area detector data. SADABS.

Che, C.M., Sun, R.W.Y. (2011). Therapeutic applications of gold complexes: lipophilic gold(III) cations and gold(I) complexes for anti-cancer treatment. Chem. Commun., (34).

Takamizawa, J., Konishi, H., Yanagisawa, K., Tomida, S., Osada, H., Endoh, H., Takahashi, T., 2004. Reduced expression of the let-7 microRNAs in human lung cancers in association with shortened postoperative survival. Cancer Res. 64 (11), 3753–3756. https://doi.org/10.1158/0008-5472.CAN-04-0637.

Team, R.C. (2013). R: A Language and Environment for Statistical Computing. R Foundation for Statistical Computing, Vienna, Austria. Retrieved from http://www.r-project.org/.

Tian, S., Siu, F.M., Kui, S.C., Lok, C.N., Che, C.M., 2011. Anticancer gold(I)-phosphine complexes as potent autophagy-inducing agents. Chem. Commun. (Camb) 47 (33), 9318–9320. https://doi.org/10.1039/c1cc11820j.

Torre, L.A., Bray, F., Siegel, R.L., Ferlay, J., Lortet-Tieulent, J., Jemal, A., 2015. Global cancer statistics, 2012. CA Cancer J. Clin. 65 (2), 87–108. https://doi.org/10.3322/caac.21262.

Wang, Z., Luo, Z., Zhou, L., Li, X., Jiang, T., Fu, E., 2015. DDX5 promotes proliferation and tumorigenesis of non-small-cell lung cancer cells by activating beta-catenin signaling pathway. Cancer Sci. 106 (10), 1303–1312. https://doi.org/10.1111/cas.12755.

Wu, F., Yuan, G., Chen, J., Wang, C., 2017. Network analysis based on TCGA reveals hub genes in colon cancer. Contemp. Oncol. (Pozn) 21 (2), 136–144. https://doi.org/10.5114/wo.2017.68622.

Xie, B., Ding, Q., Han, H., Wu, D., 2013. miRCancer: a microRNA-cancer association database constructed by text mining on literature. Bioinformatics 29 (5), 638–644. https://doi.org/10.1093/bioinformatics/btt014.